Analysis of Rapidly Twisted Hollow Waveguides

Joshua L. Wilson, *Student Member, IEEE*, Cheng Wang, Aly E. Fathy, *Fellow, IEEE*, and
Yoon W. Kang, *Senior Member, IEEE*

Abstract—**The propagation characteristics of twisted hollow waveguides are considered, and various analysis methods are proposed. It is shown that a twisted hollow waveguide can support waves that travel at a speed slower than the speed of light c. These modes are of particular interest, as slow wave structures have many potential applications in accelerators and electron traveling wave tubes. Since there is no exact closed form solution for the electromagnetic fields within a twisted waveguide or cavity, several previously proposed approximate methods are examined. It is found that the existing perturbation theory methods yield adequate results for slowly twisted structures; however, our efforts here are geared toward analyzing rapidly twisted structures using newly developed finite-difference methods. To validate the results of the theory and simulations, rapidly twisted cavity prototypes have been designed, fabricated, and measured. These measurement results are compared to simulated results, and very good agreement has been demonstrated.**

Index Terms—**Finite difference frequency domain (FDFD), finite difference time domain (FDTD), guided waves, slow wave structures.**

I. INTRODUCTION

IT IS a well known fact that straight hollow waveguides with a uniform cross section will only support modes whose phase velocity is greater than c. At the same time, many useful microwave devices depend on the interaction of charged particles with an electromagnetic (EM) wave. This is one reason why there has been interest in slow wave EM structures, which support waves traveling at speeds slower than c.

We consider a twisted waveguide, formed by extruding any cross section along a straight line while twisting. Such a waveguide is unique in that, like a straight guide, the cross section is uniform along the axis of the guide, yet unlike a straight guide, it has the capacity to support both slow and fast modes. As a result, twisted or helical structures have been considered for their application in traveling wave tubes and particle accelerators [1],[2]. Such twisted structures could potentially be easier to manufacture than other types of slow wave structures (such as dielectric loaded structures).

Analysis of twisted rectangular waveguides has been carried out before by Lewin [3] and by Yabe and Mushiake [4] and Yabe *et al.* [5]. In each of these papers, perturbation theory is used to analyze the propagation characteristics of the dominant quasi-TE mode in the waveguide. The perturbation theory approach is very well suited for analyzing the dominant TE mode in infinite twisted guides with small twist rates. However, this model is not well suited for rapidly twisted waveguides. This is because perturbation theory assumes

$$k^2 - \beta^2 = \frac{\pi^2}{a^2}\left(1 + \alpha_1 p + \alpha_2 p^2 + \cdots\right) \tag{1}$$

for some twist rate p, where all higher terms past order p^2 are dropped from the expansion. In this paper, when we speak of "slow twist rates," we refer to those cases where perturbation theory is valid, generally meaning that the product of the twist rate and the largest cross-sectional dimension is less than 1.

At high twist rates, it then becomes necessary to look beyond perturbation methods to arrive at the correct solution. In many cases, the case of rapid twist rate is of more interest in slow wave applications since rapidly twisted guides can produce more slowing of the EM wave. The perturbation theory approach also cannot take end effects into account in a twisted cavity of finite length. This could lead to errors in the calculation of the fields near the end walls of the cavity.

Therefore, it is imperative to develop new methods to analyze rapidly twisted guides. For example, it has been recently pointed out by Shyroki [6] that there exists an exact equivalent for twisted and bent waveguide structures, based on the coordinate transformation properties discussed by Nicolet *et al.* [7], [8]. Working independently of Shyroki, the authors have developed similar techniques to address this problem, and an addition to this method is presented allowing the analysis of arbitrary cross sections without the need for a staircase-type mesh. This is achieved through the use of a boundary-fitted nonorthogonal mesh [9], [10]. We also introduce a new stable 2-D nonorthogonal finite-difference time-domain (FDTD) method for solving twisted guides and present experimental verification of the results.

In this paper, we will present an overview and a mathematical description of helical geometries. From there, a coordinate transform is applied to derive three numerical methods for the solution of twisted guides: a 3-D time-domain method for simulation of twisted cavities of finite length, a 2-D time-domain method for efficient simultaneous simulation of multiple modes in an infinite twisted structure, and a 2-D frequency-domain method for individual eigenmode calculations. It is shown how these methods can be used to easily solve twisted guides of arbitrary cross section. Finally, experimental data are presented

and compared to our methods and the predictions of perturbation theory.

II. OVERVIEW OF TWISTED STRUCTURES

Twisted structures are a special case of the more general class of periodic structures. However, twisted waveguides and cavities possess certain additional properties which are not true of other periodic structures such as disk-loaded waveguides or other periodically loaded straight guides. These properties allow the transformation of the twisted structure into an equivalent straight structure with uniform cross section. The essence of the transformation is to replace the twisted (or bent) empty waveguide with a straight waveguide whose cross section is the same, but whose volume is filled with a nonuniform anisotropic material [6]. The fact that the equivalent guide is straight greatly simplifies the implementation of boundary conditions. For uniformly twisted structures, it can also be shown that the anisotropic permeability and permittivity do not involve the z coordinate. This allows much of the same machinery previously used to solve 2-D propagation problems to be brought to bear on twisted waveguide problems.

A. Defining a Twisted Geometry

Let us assume that we have a 2-D cross section defined by some implicit function of x and y. An arbitrary straight cavity can be constructed by specifying a volume

$$
\begin{aligned}
f(x, y) &< \delta \\
z_{\min} &< z < z_{\max}
\end{aligned} \tag{2}
$$

for some constant δ. It is assumed that the boundaries of the structure are perfectly conducting walls.

Now, we introduce the twisted (or helicoidal) coordinate transform employed by Lewin [3]

$$
\begin{aligned}
x' &= x \cos pz + y \sin pz \\
y' &= y \cos pz - x \sin pz \\
z' &= z.
\end{aligned} \tag{3}
$$

Here, p is some constant twist rate, usually expressed in radians per meter (Rad/m). A twisted cavity can now be defined simply by

$$
\begin{aligned}
f(x', y') &< \delta \\
z_{\min} &< z' < z_{\max}.
\end{aligned} \tag{4}
$$

It should be noted that the transverse cross section of such a helical waveguide or cavity (i.e., cut across a $z =$ constant boundary) will always yield the same shape, although rotated about the line $x = 0, y = 0$. In this sense, the structure has a uniform cross section. Fig. 1 shows an arbitrary twisted waveguide, and its corresponding straight equivalent after applying the coordinate transformation. We will first focus on twisted waveguides and cavities of rectangular cross section, and later extend the theory to arbitrary cross sections.
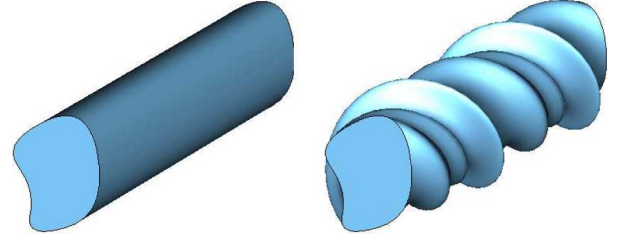

Fig. 1. Straight equivalent (*left*) to an arbitrary uniformly twisted waveguide (*right*).

B. Twisted Coordinate System

As discussed in [4], the coordinate transformation (3) is not orthogonal. Its analysis will require the covariant and contravariant basis vectors to be defined. In keeping with the conventional notation of differential geometry, we will sometimes refer to the coordinate x' as x^1, y' as x^2, and z' as x^3. The corresponding contravariant basis vectors will be denoted as e_1, e_2, and e_3, and the covariant vectors as e^1, e^2, and e^3. Following the usual convention, superscripts are used to refer to contravariant quantities, whereas subscripts are used to refer to covariant quantities. Since the coordinate system of interest is nonorthogonal, there should be no expectation that $e_i \cdot e_j = \delta_{ij}$. Instead, the covariant metric tensor must be defined

$$
g_{ij} = e_i \cdot e_j. \tag{5}
$$

For the twisted coordinate system of (3), it can be shown from basic differential geometry that

$$
[g_{ij}] = \begin{bmatrix} 1 & 0 & -py' \\ 0 & 1 & px' \\ -py' & px' & p^2(x'^2 + y'^2) + 1 \end{bmatrix}, \tag{6}
$$

from which we note that z', the transformed longitudinal coordinate, does not appear in the metric tensor. Note that as p tends to 0, $[g_{ij}]$ becomes the identity matrix, which is expected since in this case, the original Cartesian coordinate system is recovered. Following Shyroki [6] and Nicolet *et al.* [7], [8], we define a straight equivalent waveguide by loading with a nonuniform material dictated by the metric tensor

$$
\begin{aligned}
\mu^{ij} &= \mu_0 g^{ij} \sqrt{g} \\
\epsilon^{ij} &= \epsilon_0 g^{ij} \sqrt{g}.
\end{aligned} \tag{7}
$$

Here, g is the determinant of the metric tensor. g^{ij} is also the contravariant metric tensor, which is related to (6) by an inverse relationship

$$
[g_{ij}]^{-1} = [g^{ij}]. \tag{8}
$$

In this way, the problem becomes one of solving Maxwell's equations in ordinary Cartesian coordinates in a nontwisted structure, but subject to an anisotropic and nonuniform permittivity and permeability. For (6), the value of g turns out to be 1, which can often be used to simplify many expressions involving the material loading.

In the transformed (straight waveguide) problem, the components (E_x, E_y, E_z) and (H_x, H_y, H_z) are equal to the covariant components (E_1, E_2, E_3) and (H_1, H_2, H_3) in the physical problem. Note that this permittivity and permeability vary with position, but do not involve z', the transformed longitudinal coordinate. Assuming the fields can be solved in this manner, the results can be converted back into Cartesian coordinates by multiplying the appropriate Jacobian. For a detailed discussion of the mathematical foundations of the "equivalent waveguide" concept, the reader is directed to the works of Shyroki [6], Nicolet *et al.* [7], [8] and Chandezon *et al.* [11]. (Ward and Pendry [12] also made use of a similar transformation to simplify calculation of photonic Green's functions.)

III. 3-D FDTD ANALYSIS

In this section, we will apply the transformation discussed in the previous section to develop a 3-D FDTD solver. The ability to transform a twisted structure into a straight rectangular domain indicates that a finite-difference technique over a structured grid is well-suited to solve the problem, since the boundary conditions can be very simple. We developed an accurate and stable method that could be used for twisted guides. Unfortunately, a standard implementation of the FDTD technique is impossible here because, for example, in order to calculate $\boldsymbol{E}$ at any point, it is necessary to know all three components of $\boldsymbol{D}$ at that point due to the material anisotropy. In a staggered mesh this is very difficult. However, Holland [13] proposed a remedy for this situation by spatially interpolating the necessary field components. Unfortunately, this approach was found to have late-time instability problems. Schuhmann and Weiland [14] showed that this problem was due to the asymmetric evaluation of the metric tensor matrix. Their solution was to retain the spatial interpolation, but change the way the metric tensor was evaluated.

Around the same time, Thoma and Weiland [15] offered a mathematical proof for the stability of the spatial discretization method for a domain loaded with anisotropic material. Assume that the field vectors have been vectorized, and the curl operators have been appropriately discretized, leading to the well-known Maxwell grid equations (MGEs) used in the finite-integration technique [16]

$$\begin{aligned} C\boldsymbol{e} &= -\dot{\boldsymbol{b}} \\ C^T\boldsymbol{h} &= -\dot{\boldsymbol{d}} \end{aligned} \tag{9}$$

where $\boldsymbol{d}$, $\boldsymbol{e}$, $\boldsymbol{b}$, and $\boldsymbol{h}$ are the discrete vectorized representations of the fields. As mentioned in [15], the fact that the curl operator acting on the electric field is the transpose of the curl operator acting on the magnetic field is essential to the demonstration of stability. The corresponding discrete material relations are

$$\begin{aligned} \boldsymbol{d} &= D_\epsilon \boldsymbol{e} \\ \boldsymbol{b} &= D_\mu \boldsymbol{h} \end{aligned} \tag{10}$$

where D_ϵ and D_μ are matrix operators corresponding to the discretized permittivity and permeability of the material, respectively. It was shown [15] that the spatial discretization scheme is stable if the curl operators were related by a transpose as in

(9) (as mentioned earlier), and the material operators were symmetric. The late-time stability of the scheme was demonstrated theoretically (and numerically) by proving nonincreasing total field energy.

An alternative to this approach is to use the uniform unstaggered colocated mesh developed by Liu [17] and Janaswamy and Liu [18]. Forward differences are employed for the electric field, while backward differences are employed for the magnetic field. For a classic second-order scheme,

$$\begin{aligned} \frac{dE_i}{dx_j} &= \frac{E_i(x_j + h) - E_i(x_j)}{h} \\ \frac{dH_i}{dx_j} &= \frac{H_i(x_j) - H_i(x_j - h)}{h}. \end{aligned} \tag{11}$$

Liu [17] demonstrated that the dissipative errors from the forward and backward difference operators cancel each other out in such a way that the resulting wave operator is accurate to second order and has no dissipative error. It is easily demonstrated that for this mesh structure, the material operators are symmetric if the metric tensor is symmetric at every point, which is guaranteed from the definition of the metric tensor. However, a challenge presents itself around a perfectly conducting boundary since enforcing the transpose condition on the curl operators is nontrivial. This condition requires, for example, that if the computation of $(\nabla \times \boldsymbol{E})_x(i, j, k)$ involves a term $mE_y(i, j, k + 1)$ for some constant m, then the computation of $(\nabla \times \boldsymbol{H})_y(i, j, k + 1)$ must have a term $mH_x(i, j, k)$. For interior points, where (11) applies, this condition is satisfied automatically. Near a perfectly conducting boundary, the computation of $\nabla \times \boldsymbol{H}$ is typically altered to enforce the boundary condition on the electric field. If a perfectly conducting boundary exists at $i = N_x$,

$$\begin{aligned} &(\nabla \times \boldsymbol{E})_y (N_x - 1, j, k) \\ &= \frac{E_x(N_x - 1, j, k + 1) - E_x(N_x - 1, j, k)}{\Delta z} \\ &\quad - \frac{0 - E_z(N_x - 1, j, k)}{\Delta x} \\ &(\nabla \times \boldsymbol{H})_z (N_x, j, k) \\ &= \frac{H_y(N_x, j, k + 1) - H_y(N_x - 1, j, k)}{\Delta x} \\ &\quad - \frac{H_x(N_x, j, k) - H_x(N_x, j - 1, k)}{\Delta y}. \end{aligned} \tag{12}$$

Since $(\nabla \times \boldsymbol{H})_z (N_x, j, k)$ involves a term $-H_y(N_x - 1, j, k)/\Delta x$, but $(\nabla \times \boldsymbol{E})_y (N_x - 1, j, k)$ does not have a $-E_z(N_x, j, k)/\Delta x$ term, the transpose condition is not satisfied, and there is no guarantee of stability around the boundary. Clearly, another method for enforcing the boundary conditions must be implemented. To do this, a careful examination of the boundary condition is necessary around a conducting boundary, namely,

$$(\nabla \times \boldsymbol{H})_x = \frac{dD_x}{dt} = \epsilon^{1j} \frac{dE_j}{dt} = \epsilon^{11} \frac{dE_x}{dt} \tag{13}$$

for an $x =$ constant boundary, leading to the updating formula

$$\frac{dE_x}{dt} = \frac{1}{\epsilon^{11}} (\nabla \times \boldsymbol{H})_x = \frac{1}{\epsilon_0 \sqrt{g} g^{11}} (\nabla \times \boldsymbol{H})_x. \tag{14}$$

Using this relation, the material parameters can be modified along the boundary

$$[\epsilon]^{-1} = \begin{bmatrix} \dfrac{1}{\epsilon_0\sqrt{g}g^{11}} & 0 & 0 \\ 0 & 0 & 0 \\ 0 & 0 & 0 \end{bmatrix}. \tag{15}$$

Since the covariant components g_{ij} are normally computed at each mesh point, we can express g^{11} by calculating the $(1,1)$ component of $[g_{ij}]^{-1}$ and simplifying by making use of the symmetry of the metric tensor

$$[\epsilon]^{-1}$$
$$= \begin{bmatrix} \dfrac{1}{\epsilon_0\sqrt{g}}\left(g_{11} + \dfrac{g_{21}^2 g_{33} + g_{31}^2 g_{22} - 2g_{21}g_{31}g_{23}}{g_{32}^2 - g_{22}g_{33}}\right) & 0 & 0 \\ 0 & 0 & 0 \\ 0 & 0 & 0 \end{bmatrix}. \tag{16}$$

In practice, a very small number is used for the zero elements of this matrix in order to ensure that the material operator D_ϵ^{-1} remains invertible. Now, since the boundary condition around the boundary is satisfied implicitly, the expression for the curl of $\boldsymbol{E}$ around the boundary can be

$$(\nabla \times \boldsymbol{E})_y (N_x - 1, j, k)$$
$$= \frac{E_x(N_x - 1, j, k+1) - E_x(N_x - 1, j, k)}{\Delta z}$$
$$- \frac{E_z(N_x, j, k) - E_z(N_x - 1, j, k)}{\Delta x} \tag{17}$$

satisfying the transpose condition and ensuring stability. This modification of the material parameters around a conducting boundary in an unstaggered collocated nonorthogonal FDTD scheme to ensure stability is novel to this approach, and has not been done by others.

With the material matrices derived in this fashion and using the normal Cartesian curl operators, the grid equations of (9) can be updated at each time step using an appropriate time integrator (such as leap frog for a second-order scheme). The result is a scheme rather similar to the nonorthogonal FDTD method [13], but not subject to the troubling late-time instability phenomena. The Courant stability criteria for the time step cannot be expressed by a simple formula, as was the case for rectangular grids. However, an upper bound can be set using formulas given in [19]. The authors have designed both second-order schemes (employing classic second-order spatial differences and leap frog time integration) and fourth-order schemes (employing a fourth-order spatial difference operator and RK4 based time integration). In both cases, stable and efficient operation has been achieved.

To check the late-time numerical stability, the total cavity energy was computed over time for a simulation of a twisted rectangular cavity (the one discussed later in this paper). The results can be shown in Fig. 2 for up to 8×10^6 time steps. Although the total energy can be seen to fluctuate over time, no late-time instability has ever been observed with this technique, either with a second- or fourth-order implementation. The energy fluctuations are due to the inherent error of the time integrator, as
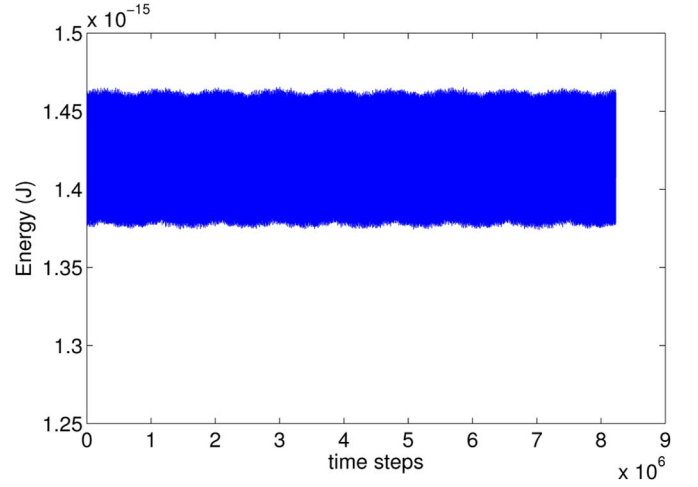

Fig. 2. Cavity energy versus time showing late time stability of the proposed 3-D scheme.

evidenced by the fact that the fluctuations can be reduced arbitrarily by decreasing the time step and/or using a higher order integrator such as RK4.

The 3-D solver is excellent for solving twisted cavities of finite length. However, for solving infinite twisted guides (or even very long twisted cavities where end effects can be neglected), the algorithm can be made much more efficient by using a 2-D mesh, rather than a 3-D one.

IV. 2-D FINITE-DIFFERENCE ANALYSIS

As mentioned previously, the twisted structure is a specific type of periodic structure so it is natural to turn to solvers that use periodic boundary conditions. However, for the twisted guide, the algorithm can be simplified much further since the period can essentially be reduced to zero if the appropriate coordinate system is chosen, giving a 2-D mesh in the limiting case.

A 2-D finite-element solver for TE modes in twisted waveguides was proposed by Igarashi and Honma [20]. This solver works well for slowly twisted guides, where the modes can still be regarded as basically TE or TM independently. Strictly speaking, however, TE and TM modes do not exist in a twisted waveguide (as shown by Yabe and Mushiake [4]). A hybrid mode is needed to satisfy the boundary conditions, and this becomes particularly critical as the twist rate becomes relatively large and there is significant deviation from the straight waveguide case. Therefore, we applied finite-difference techniques to the straight waveguide equivalent problem. (A finite element approach also using the straight equivalent can be found in [21].)

A 2-D FDTD algorithm for the efficient solution of straight waveguide propagation problems was proposed by Xiao *et al.* [22]. This should not be confused with the conventional 2-D FDTD method where the fields are assumed to be uniform in one direction. Here, the idea is to assume a complex solution of the form

$$E = E_1(x, y, t)e^{-j\beta z}$$
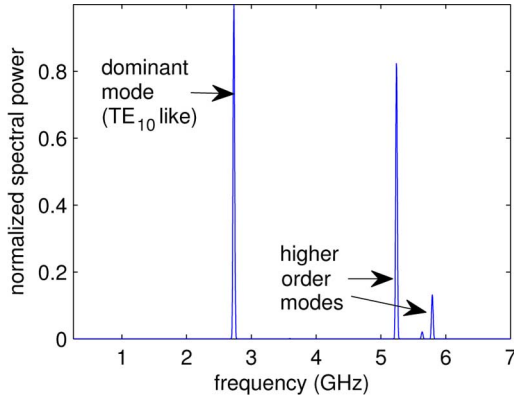$$H = H_1(x, y, t)e^{-j\beta z}. \tag{18}$$

Fig. 3.   Sample spectrum obtained by 2-D time-domain simulation of a twisted rectangular guide.

Here, we are solving only one traveling wave mode solution of the twisted guide problem at a time. Any such modes can exist independently since they perfectly satisfy the boundary conditions. Instead of the z derivatives being calculated in the conventional sense using finite differences, they are calculated by multiplying that field component by $-j\beta$. In this manner, the quantities E_1 and H_1 can be updated using a time integrator. Although this means that the computations will now involve complex quantities rather than the purely real computations of the classical FDTD method, the mesh can be reduced from three dimensions to two. A simple uniform mesh can be used if the material properties are modified around the conducting boundary surface, as discussed above.

A.   Time-Domain Implementation

Assuming field solutions of the form (18), a time-domain solver can easily be derived using the same uniform mesh concept employed for the 3-D case, but reduced to two dimensions. The real time-domain fields at any point (x, y, z) in the equivalent straight structure can be recovered from the complex solution using

$$E(x,y,z,t) = \Re\{E_1(x,y,t)e^{-j\beta z}\}$$
$$H(x,y,z,t) = \Re\{H_1(x,y,t)e^{-j\beta z}\}. \qquad (19)$$

$\Re\{\}$ represents the real part. The value of β is a running variable from 0 to ∞. Each value of β will result in a number of modes with different frequencies. This technique allows dispersion curves to be obtained efficiently for a large number of modes. We do this by running a number of simulations while sweeping the value of β. A multimode initial condition is used, and a fast Fourier transform (FFT) is performed on the output fields of each simulation to obtain the frequencies of the modes.

A sample spectrum obtained by 2-D time-domain analysis of a twisted rectangular waveguide is shown in Fig. 3. As previously mentioned, a mixed-mode initial condition was purposefully chosen to produce a broad spectrum of excited modes. Like the 3-D method we developed, there was no late-time instability observed in the results produced by this method. The mode with the lowest frequency is the dominant TE-like mode that is investigated experimentally later in this paper.

We demonstrated that a 2-D time-domain method can be used to solve for the fields and the frequencies of many modes in a rapidly twisted structure over a wide range of frequencies simultaneously. However, the time-domain solver is not capable of directly extracting the eigenmodes of the twisted waveguide, so we also discuss an implementation in the frequency domain.

B.   Frequency-Domain Implementation

The finite-difference frequency-domain (FDFD) method has been discussed by Lui and Chen [23]. In it, the fields are assumed to be harmonic in time and in the z direction so the explicit time updating scheme of the FDTD method is eliminated completely and replaced by an eigenvalue problem. In it, all six field components are solved for directly. Later, it was found that the number of actual solved field components and the number of nonzero matrix elements could be reduced significantly [24], [25]. The solution of curved waveguides using 2-D FDFD has previously been attempted by Lavranos and Kyriacou [26]. However, their formulation depended on an orthogonal coordinate system and the ability to separate the field into axial and transverse components, which was mentioned in [26] to be invalid for high curvature rates (or small curvature radii). Thus, the extension of their work to rapidly twisted waveguides is problematic.

By contrast, this research proposes to solve the twisted structure in nonorthogonal coordinates which is based on an exact equivalent, and does not make any simplifying assumptions that would be invalid for high twist rates. To use this method to solve the Maxwell equations for a twisted waveguide structure, the vector Helmholtz equation in general curvilinear coordinates is derived. Upon substitution of (7) into the Maxwell curl equations, we have

$$\frac{1}{\sqrt{g}}[g_{ij}]\nabla \times E = -j\omega\mu_0 H \qquad (20)$$

$$\frac{1}{\sqrt{g}}[g_{ij}]\nabla \times H = j\omega\epsilon_0 E \qquad (21)$$

which leads to the eigensystem

$$\frac{1}{\sqrt{g}}[g_{ij}]\nabla \times \left(\frac{1}{\sqrt{g}}[g_{ij}]\nabla \times E\right) = k_0^2 E. \qquad (22)$$

In this scheme, three vector components have to be computed at each grid point. For example, if a 20×20 grid was employed to solve a twisted square waveguide, the dimension of the system would be $20 \times 20 \times 3 = 1200$, and the total number of matrix elements would be $1200^2 = 1.44 \times 10^6$. Fortunately, the use of finite differences assures us that the matrix will likely be sparse. If the sparsity of the matrix is taken into account, it can drastically reduce memory and calculation time. If the field components are vectorized as in the MGEs, the same matrix operators can be used to calculate both the frequency- and time-domain solutions. It is difficult to give a definitive rule regarding how many mesh points are needed for a good simulation. In general, it will depend greatly on the judicious choice of a structured mesh. In practice, one should run several cases with varying degrees of mesh refinement to determine when convergence has been achieved.
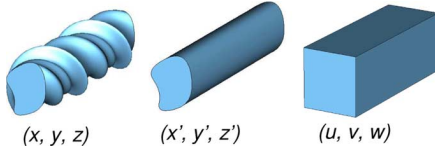
Fig. 4. Cascaded coordinate transformation used to analyze arbitrary twisted structures.

V. TWISTED GUIDES OF ARBITRARY CROSS SECTION

Thus far, we have only considered twisted waveguides of rectangular cross section. Fortunately, our choice of a twisted coordinate system allows a simple cascaded coordinate transform that permits a solution to arbitrary twisted guides. The coordinate transform of (3) is combined with a planar transform

$$
\begin{aligned}
x' &= x'(u,v) \\
y' &= y'(u,v) \\
z' &= w.
\end{aligned}
\tag{23}
$$

The coordinates (u,v,w) are arranged in a Cartesian grid. This cascaded transform is illustrated in Fig. 4. The functions u and v can be derived using finite differences from any commercial or freeware software package capable of generating 2-D structured planar meshes. The authors have made use of a free utility called UNAMALLA to generate such meshes [27]. The covariant metric tensor for this cascaded transform can be obtained using the rule

$$
(g_{ij})_u = (g_{mn})_{x'} \frac{\partial x'^m}{\partial u^i} \frac{\partial x'^n}{\partial u^j}.
\tag{24}
$$

Here, $(g_{mn})_{x'}$ is the metric tensor for the transform from Cartesian coordinates to the primed coordinates [in this case, (3)], and the labels u^i correspond to (u,v,w). Under this transformation,

$$
[g_{ij}] = \begin{bmatrix} x_u'^2 + y_u'^2 & x_u'x_v' + y_u'y_v' & px'y_u' - py'x_u' \\ x_u'x_v' + y_u'y_v' & x_v'^2 + y_v'^2 & px'y_v' - py'x_v' \\ px'y_u' - py'x_u' & px'y_v' - py'x_v' & 1 + p^2(x'^2 + y'^2) \end{bmatrix}.
\tag{25}
$$

Also, note again that the longitudinal coordinate does not appear in the metric tensor, allowing 2-D methods to be used. Since typical mesh generation programs output the coordinates of each point on the grid, x' and y' are known at each mesh point. The derivatives x_u', x_v', y_u', and y_v' are calculated using finite differences. From here, the relations of (7) can be used to calculate the material properties of the transformed guide.

One particular case of interest in slow wave applications is the twisted "keyhole" structure, whose longitudinal cross section is identical to a disk loaded waveguide. The cross section, along with the generated UNAMALLA mesh, is shown in Fig. 5. This twisted structure is similar to the "helical groove waveguide" discussed by Flouds and Mansell [28], which has application in traveling wave tubes. (In fact, the present theory also provides a method for accurately solving that structure as well.)

VI. COMPARISON AND DISCUSSION

In this section, an example twisted rectangular waveguide is considered. The waveguide has cross-sectional dimensions of
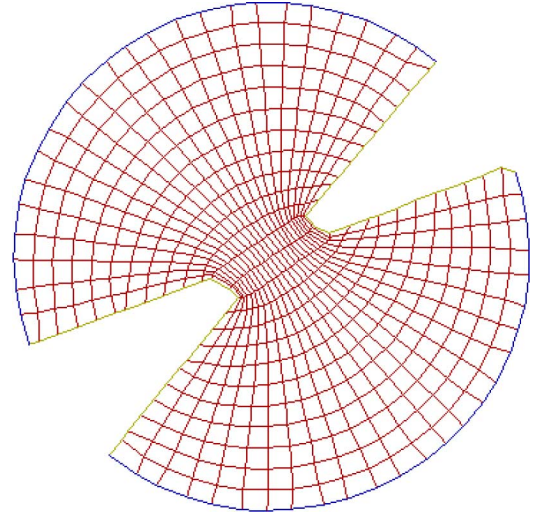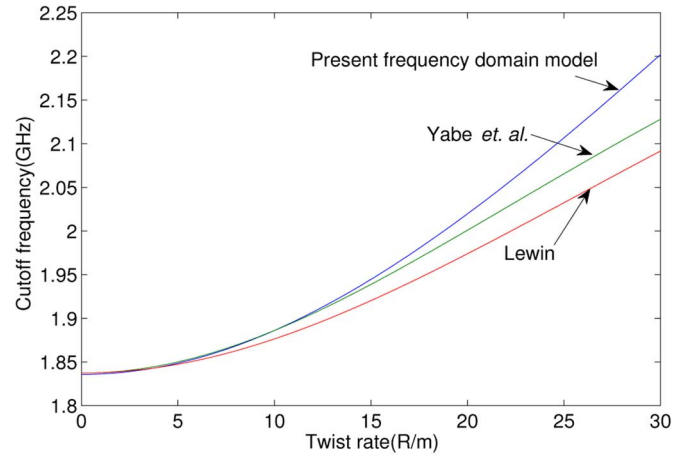

Fig. 5. Keyhole cross section and corresponding mesh.

Fig. 6. Cutoff frequencies predicted for 8.16 cm $\times$ 3.63 cm rectangular waveguide.

8.16 cm $\times$ 3.63 cm. We will use this case to discuss the results of the present numerical methods in light of the findings of Lewin, Yabe, Nishio, and Mushiake. To determine at what value of twist rate there is significant deviation, we calculate the expressions given in [5] for Lewin's theory and that presented by Yabe *et al.* The cutoff frequencies predicted by these two perturbation methods are compared to the results of the developed 2-D FDFD method, employing a 50×50 grid. The finite-difference calculation was done using MATLAB on a 1.86-GHz Intel Core 2 CPU. Calculating the first five eigenmodes took 14 s and used roughly 55 MB of memory. The comparison to perturbation theory is shown in Fig. 6.

For low values of twist rate, all three theories are found to be in excellent agreement. As the twist rate increases, however, the results of Lewin begin to be less accurate than those of Yabe *et al.* This is because Lewin formulated his theory assuming simple TE waveguide modes, whereas the more accurate theory presented by Yabe *et al.* assumes a hybrid mode which satisfies the boundary conditions of the twisted guide. Measurement results were given in [5], and these showed good experimental

agreement at low twist rates. If the waveguide structures measured in Yabe's paper are scaled up to the same physical size as the waveguides investigated here, the twist rates are all below 13 Rad/m. Fig. 6 shows that at this twist rate, the theory of [5] is still in close agreement with the finite-difference method presented here.

However, as the twist rate becomes even more rapid, all perturbation methods appear to be inadequate. This phenomenon explains the drastic difference between the perturbation theory predictions and our measured results for the rapidly twisted rectangular cavity. This result is to be expected since perturbation theory neglects higher order correction terms for rapid twists. In order to verify the accuracy of the methods applied to rapidly twisted structures, it becomes necessary to turn to commercial software (such as HFSS or CST) or experimental validation.

VII. EXPERIMENTAL VERIFICATION

To validate the developed 3-D finite-difference method, a twisted rectangular cavity prototype with the same cross-sectional dimensions as in the previous section was designed to work near 2.8 GHz. The cavity has two complete twists over a length of 22.7 cm. For this case, ($p = 55.4$ Rad/m), Fig. 6 shows that perturbation methods clearly will not suffice. The prototype was printed using a stereolithography apparatus (SLA) technique and then copper plated on the inside. This method can allow the rectangular cross section to be accurately preserved even for large twist rates. Fig. 7 shows the completed prototype. This particular prototype was selected because of its moderately high twist rate, enabling the accuracy of the newly proposed methods to be compared with the existing perturbation theory method.

Measurements were taken on this prototype by placing a copper plate on each end of the waveguide, effectively turning it into a resonant cavity. Two small probes were inserted in the end plates, and a vector network analyzer was used to measure the transmission coefficient S_{21} over a wide range of frequencies. The maxima of $|S_{21}|$ correspond to the resonant modes of the cavity structure. Fig. 8 shows S_{21} over the range of frequencies spanning the first four TE-like modes of the resonant cavity. The frequencies and Q values for these modes are shown in Table I.

Since the cavity is rather electrically short, end effects were found to limit the effectiveness of the 2-D code for this case. A straight rectangular waveguide can be converted into a cavity by introducing shorting plates without affecting the eigenmodes (since the tangential electric field of TE modes in the waveguide naturally vanishes each half cycle). Unfortunately the same cannot be said of a twisted rectangular guide so some perturbation in the mode will be introduced by the metal wall.

An $18 \times 8 \times 50$ grid was employed for the 3-D solver, and the simulation was allowed to run to 50 ns. The phase constant was selected by establishing an initial condition that contained a particular number of half-cycle variations in the longitudinal direction. The frequency of the resonant mode was then obtained through the use of an FFT. These frequencies were then compared to the measured frequencies and found to be within 0.5% of each other. By comparison, the error using the perturbation
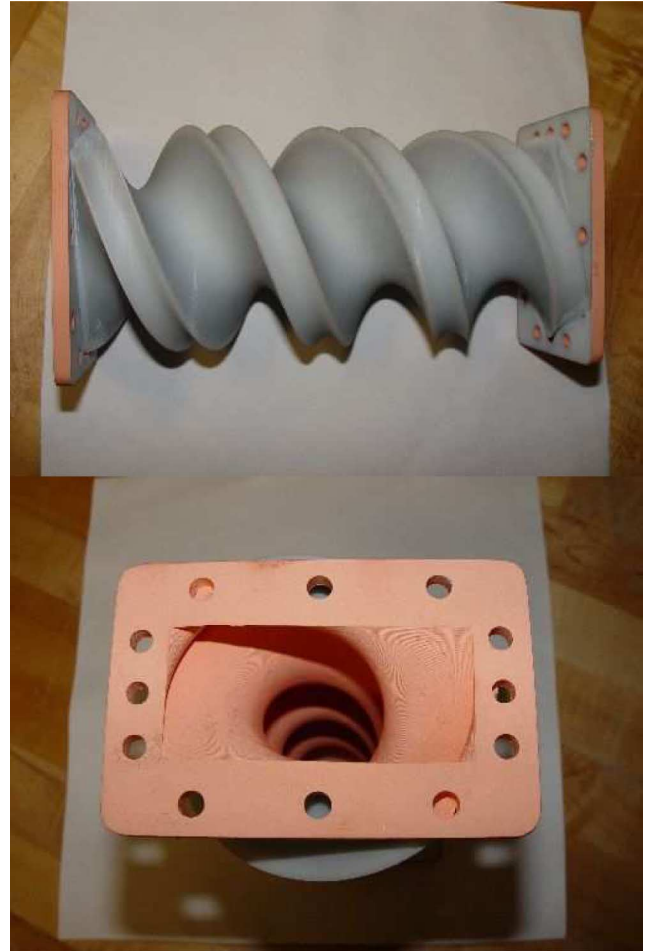

Fig. 7.   Twisted rectangular waveguide prototype.
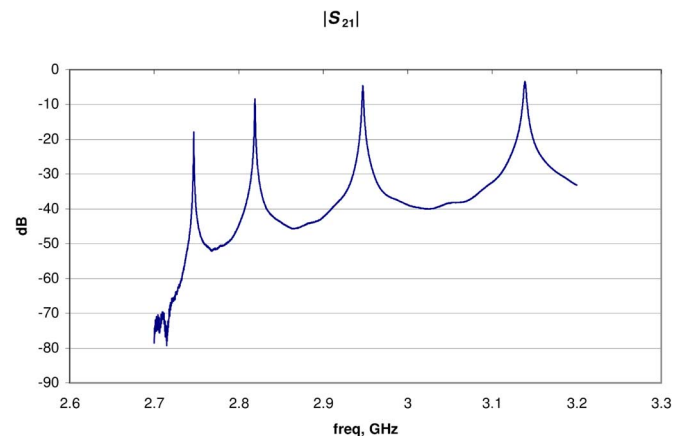
Fig. 8.   Measured $|S_{21}|$ for the short twisted rectangular prototype showing resonances.

theory equations given by Yabe *et al.* in [5] was more than 8% for each of the modes.

For the 2-D method, using a 72×32 2-D mesh, the code yielded up to 1.8% frequency deviation from experiment. Again, the 2-D code solves the structure as if it were infinite. Therefore, to further validate the effectiveness of the 2-D code, another prototype was constructed that was identical to the first,

TABLE I
EXPERIMENTALLY MEASURED FIRST FOUR TE-LIKE MODES FOR THE SHORT TWISTED
RECTANGULAR PROTOTYPE COMPARED TO 3-D SIMULATION RESULTS

	Measured frequency	**Q**	Simulation Frequency (3D FDTD)	Deviation from Experiment
Mode 1	2.747 GHz	7001	2.734 GHz	0.47%
Mode 2	2.820 GHz	3977	2.808 GHz	0.43%
Mode 3	2.947 GHz	1921	2.940 GHz	0.24%
Mode 4	3.139 GHz	1003	3.135 GHz	0.13%

TABLE II
SHORT AND LONG PROTOTYPE RESONANT FREQUENCIES
COMPARED TO 2-D SIMULATION METHOD RESULTS

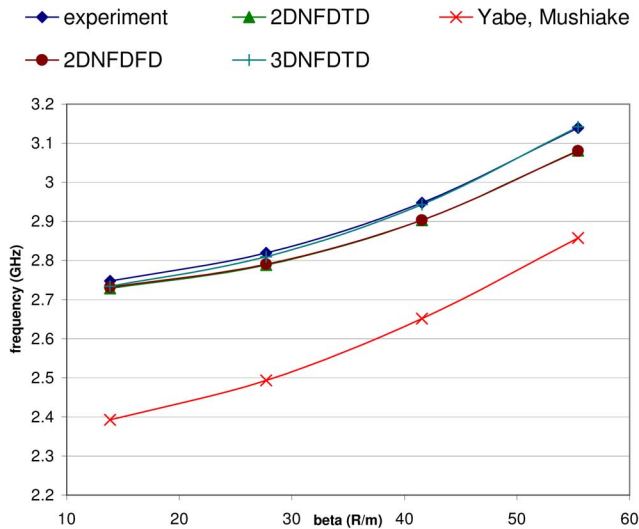| Short Prototype Frequency	Long Prototype Frequency	2DNFDTD	2DNFDFD
2.747 GHz	2.743 GHz	2.734 GHz	2.735 GHz
2.820 GHz	2.808 GHz	2.794 GHz	2.794 GHz
2.947 GHz	2.932 GHz	2.907 GHz	2.906 GHz
3.139 GHz	3.119 GHz	3.083 GHz	3.082 GHz

Fig. 9. Dispersion curves showing measured and predicted resonant frequencies for twisted rectangular cavity (beta is the phase constant).
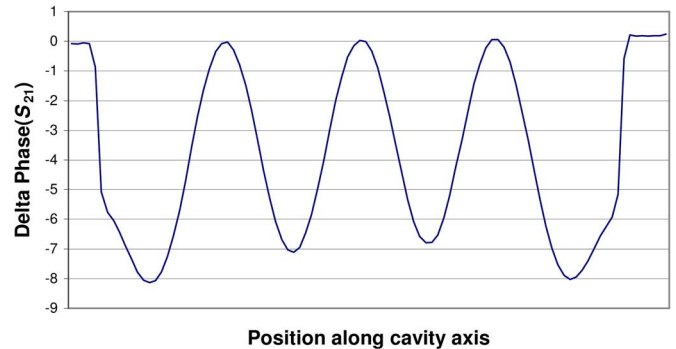

Fig. 10. Bead-pull measurement of a 2.8-GHz TM mode of the "keyhole" twisted structure.

traveling wave tubes in which particles move at relativistic velocities extremely close to the speed of light. The measured frequency was 2.8135 GHz. For a 25×25 grid, the 2-D frequency-domain method yielded a resonant frequency of 2.8159 GHz, while the 2-D time-domain method gave 2.8158 GHz. The fact that the measured results are very close to prediction indicates that for this TM mode, the perturbations caused by the end walls are small (at least for that value of twist rate).

In order to ensure that the mode measured was indeed the mode predicted by the model, the phase constant was measured and compared with the β value used in the simulation. Here, the mode of interest has two complete cycles over the length of the cavity for an expected $\beta = 59.84$ Rad/m. To experimentally measure β, a bead-pull measurement was performed to measure the magnitude of the electric field on the axis of the guide. In this perturbational technique, a probe is placed at each end of the cavity. The transmission is measured at the resonant frequency while a small metallic bead is passed along the cavity axis. The very small shift in resonant frequency (measured as a change in the phase of the transmission) is proportional to the square of the magnitude of the electric field at the bead position. The interested reader is directed to [29] and [30] for a detailed discussion of this well-known method.

The results of the bead pull are shown in Fig. 10. The horizontal axis shows the bead position along the axis. The plot reveals four distinct minima in the phase of the transmission (corresponding to maxima in the electric field strength). This is consistent with the expectation that the resonant mode has two complete cycles over the cavity length. The small difference between the two middle peaks is likely due to measurement error.

The cavity was also simulated in CST Microwave Studio (version 2006) [31] (a commercial EM simulation tool which can perform well for slow to moderate twist rates). The predicted resonant frequency was 2.817 GHz, very close to the measured

except twice as long, now with four complete twists. The measurement results for the short and long cavities as well as the 2-D NFDTD and 2-D NFDFD results are shown in Table II.

The trend in the experimental results of Table II indicates that as the cavity gets physically longer, the measured resonant frequency approaches the predictions of the 2-D methods, as expected. In the limiting case of an infinite structure, end effects should become negligible, and it is expected that the 2-D method will perform quite well.

The experimental cavity results were used to generate dispersion curves. These are compared to the various simulation methods we developed in Fig. 9.

To test the 2-D methods for twisted guides of arbitrary cross section, a keyhole cross section was defined in the transverse plane, as in Fig. 5. Since this structure has potential application for particle acceleration purposes, a TM mode near 2.8 GHz was chosen for analysis. A prototype was constructed with three complete twists over a length of 21 cm. This particular design was chosen so that the phase velocity of the wave would be exactly c, which is necessary for most electron accelerators and
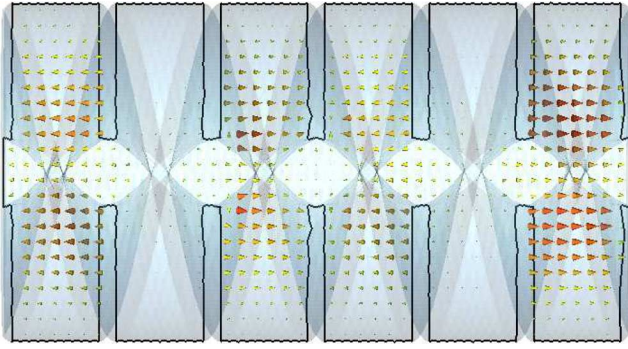
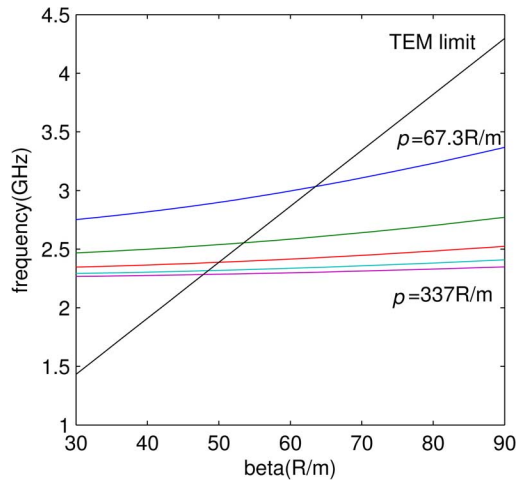Fig. 11. CST simulation of the "keyhole" twisted structure.

Fig. 12. Predicted dispersion curves of the "keyhole" twisted structure using the 2-D frequency-domain method for varying twist rates.

resonant frequency. The electric field is shown in Fig. 11, which indicates four maxima in the magnitude of the electric field along the cavity axis, just as measured in the bead pull. The measured phase velocity, calculated from the measured resonant frequency and phase constant, is 2.95×10^8 m/ s. This offers great practical promise since many disk loaded structures with similar longitudinal cross section to this twisted structure are designed to accelerate electrons at near relativistic velocities. Both the CST results and the bead-pull measurements indicate that the intensity of the electric field increases close to the end walls of the cavity. This is to be expected since these walls will cause a perturbation of the mode that would otherwise exist in an infinite twisted waveguide. The 3-D method must be used if the effects of the end walls cannot be neglected. Analysis of the TM accelerating mode using the proposed techniques is very efficient. For example, using the 2-D frequency-domain technique, calculation of each mode for a 25×25 grid takes less than 1 s on a 1.86-GHz Intel processor running MATLAB. This allows detailed studies to be performed regarding the dispersion characteristics of a twisted guide, among other things. For this "keyhole" design, the dispersion curves for a variety of twist rates is shown in Fig. 12. It is interesting to note that unlike a TE mode in a twisted rectangular guide, the cutoff frequency is seen to decrease as the twist rate increases. Perturbation theory

applied to the dominant mode of a twisted rectangular guide predicts the opposite effect (i.e., an increase of the cutoff frequency with increasing twist rate) [5]. This gives one example of how the present method can be readily applied to do very rapid design and optimization of twisted slow wave structures. In addition to dispersion information, other useful figures of merit can be extracted from the eigenmodes of the 2-D frequency-domain solutions.

VIII. CONCLUSION

The problem of rapidly twisted structures has been analyzed in detail. The existing perturbation theory methods were found to be quite accurate for low twist rates, but faster twist rates required new models to be developed. Efficient 3-D and 2-D numerical techniques have been proposed to solve this problem. These methods are based on an exact straight equivalent waveguide with anisotropic permittivity and permeability that do not vary along the longitudinal direction. This uniformity along the axis of the twisted guide enables the use of conventional 2-D nonorthogonal FDTD and FDFD solvers.

This work expands the previous work done by Shyroki [6] by treating arbitrary cross sections without the need for a staircase-type mesh and developing a stable 2-D (and 3-D) nonorthogonal FDTD method to solve twisted guides. Arbitrary cross sections can be analyzed simply using these techniques if a 2-D structured grid can be created. In addition, good agreement with experimental measurements has been achieved. Moreover, the contributions of end effects to the twisted cavities are investigated experimentally by constructing both long and short twisted prototypes. The experimental data suggests that the 2-D methods in both the time and frequency domain become accurate when the twisted structure is very long.

The accuracy and efficiency of these methods will provide an attractive way of designing slow wave structures for accelerators and traveling wave tubes. It is possible to predict accurately the slowing of the EM wave, the dispersion relationship, mode characteristics, and higher order modes for such devices. The reduced complexity of these methods circumvents meshing problems associated with existing numerical solvers for very rapidly twisted geometries. As a result, the solutions are obtained in a very efficient fashion.

REFERENCES

[1] W. Wang, G. Yu, and Y. Wei, "Study of the ridge-loaded helical-groove slow-wave structure," *IEEE Trans. Microw. Theory Tech.*, vol. 45, no. 10, pp. 1689–1695, Oct. 1997.

[2] Y. W. Kang, "Twisted waveguide accelerating structure," presented at the 9th Adv. Accelerator Concepts Workshop, Aug. 2000.

[3] L. Lewin, *Theory of Waveguides*. London, U.K.: Newness–Butherworths, 1975.

[4] H. Yabe and Y. Mushiake, "An analysis of a hybrid-mode in a twisted rectangular waveguide," *IEEE Trans. Microw. Theory Tech.*, vol. MTT-32, no. 1, pp. 65–71, Jan. 1984.

[5] H. Yabe, K. Nishio, and Y. Mushiake, "Dispersion characteristics of twisted rectangular waveguides," *IEEE Trans. Microw. Theory Tech.*, vol. MTT-32, no. 1, pp. 91–96, Jan. 1984.

[6] D. Shyroki, "Exact equivalent straight waveguide model for bent and twisted waveguides," *IEEE Trans. Microw. Theory Tech.*, vol. 56, no. 2, pp. 414–419, Feb. 2008.

[7] A. Nicolet, F. Zolla, and S. Guenneau, "Modelling of twisted optical waveguides with edge elements," *Eur. Phys. J. Appl. Phys.*, vol. 28, pp. 153–157, 2004.

[8] A. Nicolet, F. Zolla, Y. Agha, and S. Guenneau, "Leaky modes in twisted microstructured optical fibers," *Waves in Random Complex Media*, vol. 17, no. 4, pp. 559–570, Nov. 2007.

[9] A. J. Ward and J. B. Pendry, "Refraction and geometry in Maxwell's equations," *J. Modern Opt.*, vol. 43, pp. 773–793, 1996.

[10] D. Shyroki, "Efficient Cartesian-grid-based modeling of rotationally symmetric bodies," *IEEE Trans. Microw. Theory Tech.*, vol. 55, no. 6, pp. 1132–1138, Jun. 2007.

[11] J. Chandezon, D. Maystre, and G. Raoult, "A new theoretical method for diffraction gratings and its numerical application," *J. Opt.*, vol. 11, no. 4, pp. 235–241, 1980.

[12] A. J. Ward and J. B. Pendry, "Calculating photonic Green's functions using a nonorthogonal finite-difference time-domain method," *Phys. Rev. B, Condens. Matter*, vol. 58, no. 11, pp. 7252–7259, Sep. 1998.

[13] R. Holland, "Finite-difference solutions of Maxwell's equations in generalized nonorthogonal coordinates," *IEEE Trans. Nucl. Sci.*, vol. 30, no. 6, pp. 4589–4591, Dec. 1993.

[14] R. Schuhmann and T. Weiland, "Stability of the FDTD algorithm on nonorthogonal grids related to the spatial interpolation scheme," *IEEE Trans. Magn.*, vol. 34, no. 5, pp. 2751–2754, Sep. 1998.

[15] P. Thoma and T. Weiland, "Numerical stability of finite difference time domain methods," *IEEE Trans. Magn.*, vol. 34, no. 5, pp. 2740–2743, Sep. 1998.

[16] T. Weiland, "Time domain electromagnetic field calculation with finite difference methods," *Int. J. Numer. Modeling*, vol. 9, pp. 295–319, 1996.

[17] Y. Liu, "Fourier analysis of numerical algorithms for the Maxwell equations," *J. Comput. Phys.*, vol. 124, no. 2, pp. 396–416, Mar. 1996.

[18] R. Janaswamy and Y. Liu, "An unstaggered colocated finite-difference scheme for solving time-domain Maxwell's equations in curvilinear coordinates," *IEEE Trans. Antennas Propag.*, vol. 45, no. 11, pp. 1584–1591, Nov. 1997.

[19] J.-F. Lee, R. Palandech, and R. Mittra, "Modeling three-dimensional discontinuities in waveguides using nonorthogonal FDTD algorithm," *IEEE Trans. Microw. Theory Tech.*, vol. 40, no. 2, pp. 346–352, Feb. 1992.

[20] H. Igarashi and T. Honma, "A finite element analysis of TE modes in twisted waveguides," *IEEE Trans. Magn.*, vol. 27, no. 5, pp. 4052–4055, Sep. 1991.

[21] A. Nicolet and F. Zolla, "Finite element analysis of helicoidal waveguides," *IET Sci., Meas., Technol.*, vol. 1, no. 1, pp. 67–70, Jan. 2007.

[22] S. Xiao, R. Vahldieck, and H. Jin, "Full-wave analysis of guided wave structures using a novel 2-D FDTD," *IEEE Microw. Guided Wave Lett.*, vol. 2, no. 5, pp. 165–167, May 1992.

[23] M.-L. Lui and Z. Chen, "A direct computation of propagation constant using compact 2-D full-wave eigen-based finite-difference frequency domain technique," in *Proc. Int. Comput. Electromagn. Appl. Conf.*, 1999, pp. 78–81.

[24] Y.-J. Zhao, K.-L. Wu, and K.-K. M. Cheng, "A compact 2-D full-wave finite-difference frequency-domain method for general guided wave structures," *IEEE Trans. Microw. Theory Tech.*, vol. 50, no. 7, pp. 1844–1848, Jul. 2002.

[25] Li L.-Y and J.-F. Mao, "An improved compact 2-D finite-difference frequency-domain method for guided wave structures," *IEEE Microw. Wireless Compon. Lett.*, vol. 13, no. 12, pp. 520–522, Dec. 2003.

[26] C. S. Lavranos and G. A. Kyriacou, "A finite difference frequency domain study of curvature lifted modes degeneration," in *Progr. Electromagn. Res. Symp.*, Aug. 27–30, 2007, pp. 222–226.

[27] P. Barrera, G. Gonzalez, L. Castellanos, and A. Prez, UNAMALLA Mesh Generation Package May 2008. [Online]. Available: http://www.mathmoo.unam.mx/unamalla

[28] K. H. Flouds and J. R. Mansell, "Propagation of an electronic wave through a helical waveguide," *Proc. Inst. Elect. Eng.*, vol. 3, no. 11, pp. 1789–1798, 1964.

[29] L. Maier and J. Slater, "Field strength measurements in resonant cavities," *J. Appl. Phys.*, vol. 23, no. 1, pp. 68–77, Jan. 1952.

[30] D. Goldberg and R. Rimmer, "Measurement and identification of homs in RF cavities," in *Proc. Particle Accelerator Conf.*, May 12–16, 1997, vol. 3, pp. 3001–3003.

[31] *"CST Microwave Studio 2006 User's Manual,"* CST Ltd., Darmstadt, Germany, 2006.

Joshua L. Wilson (S'07) received the B.S.E.E. degree in electrical engineering from Marquette University, Milwaukee, WI, in 2004, and the Ph.D. degree in EM theory from the University of Tennessee, Knoxville, in 2008.

While working toward the Ph.D. degree at the University of Tennessee, he conducted research related to charged particle accelerator systems at the Spallation Neutron Source (SNS) project at Oak Ridge National Laboratory (ORNL), Oak Ridge, TN.

Cheng Wang received the Ph.D. in mathematics from Temple University, Philadelphia, PA, in 2000.

He has been actively involved with research on the numerical simulation of partial differential equations and corresponding physical applications.

Aly E. Fathy (S'82–M'84–SM'92–F'04) received the B.S.E.E. degree, B.S. degree in pure and applied mathematics, and M.S.E.E. degree from Ain Shams University, Cairo, Egypt, in 1975, 1979, and 1980, respectively, and the Ph.D. degree from the Polytechnic Institute of New York, Brooklyn, in 1984.

In February 1985, he joined the RCA Research Laboratory (currently the Sarnoff Corporation), Princeton, NJ, as a Member of the Technical Staff. In 2001, he became a Senior Member of the Technical Staff. While with the Sarnoff Corporation, he was engaged in the research and development of various enabling technologies such as high-Tc superconductors, low-temperature co-fired ceramic (LTCC), and reconfigurable holographic antennas. He was also an Adjunct Professor with the Cooper Union School of Engineering, New York, NY. In August 2003, he joined the University of Tennessee, Knoxville, as an Associate Professor. He has authored or coauthored numerous transactions and conference papers. He holds 11 U.S. patents. His current research interests include wireless reconfigurable antennas, see-through walls, ultra-wideband (UWB) systems, and high-efficiency high-linearity combining of digital signals for base-station amplifiers. He has developed various microwave components/subsystems such as holographic reconfigurable antennas, radial combiners, direct broadcast antennas (DBSs), speed sensors, and LTCC packages for mixed-signal applications.

Dr. Fathy is a member of Sigma Xi and Eta Kappa Nu. He is an active member of the IEEE Microwave Theory and Techniques Society (IEEE MTT-S) International Microwave Symposium (IMS) Technical Program Committee (TPC), the IEEE Antenna and Propagation Symposium, and the IEEE Radio and Wireless Steering Committee. He was the Technical Program chair of the 2008 IEEE Radio Wireless Conference. He was the recipient of five Sarnoff Outstanding Achievement Awards (1988, 1994, 1995, 1997, 1999).

Yoon W. Kang (S'83–M'87–SM'04) was born in Seoul, Korea, on January 12, 1950. He received the B.E. degree in electrical engineering from Yonsei University, Seoul, Korea, in 1972, the M.S. degree in electrical engineering from the University of California at Santa Barbara, in 1982, and the Ph.D. degree in electrical engineering from the University of Massachusetts at Amherst, in 1986.

From 1974 to 1980, he was a Microwave Systems Engineer with the Agency for Defense Development of Korea. From 1986 to 1991, he was with the Medical Systems Group, General Electric Company, Waukesha, WI, and then with the Astrospace Division, General Electric Company, Princeton, NJ, where he was involved with magnetic resonance imaging systems and satellite communication systems, respectively. From 1991 to 2000, he was involved with various charged particle accelerators and related systems with the Advanced Photon Source project at the Argonne National Laboratory, Argonne, IL. Since 2000, he has been involved with the Spallation Neutron Source (SNS) project at the Oak Ridge National Laboratory (ORNL), Oak Ridge, TN.